UNIVERSITY OF AMSTERDAM

UvA-DARE (Digital Academic Repository)

Discovery of Psr J1227-4853: A Transition from a Low-mass X-Ray Binary to a Redback Millisecond Pulsar

Roy, J.; Ray, P.S.; Bhattacharyya, B.; Stappers, B.; Chengalur, J.N.; Deneva, J.; Camilo, F.; Johnson, T.J.; Wolff, M.; Hessels, J.W.T.; Bassa, C.G.; Keane, E.F.; Ferrara, E.C.; Harding, A.K.; Wood, K.S.

Link to publication

DISCOVERY OF PSR J1227−4853: A TRANSITION FROM A LOW-MASS X-RAY BINARY TO A REDBACK MILLISECOND PULSAR

Jayanta Roy[1,2], Paul S. Ray[3], Bhaswati Bhattacharyya[1], Ben Stappers[1], Jayaram N. Chengalur[2], Julia Deneva[4], Fernando Camilo[5], Tyrel J. Johnson[6], Michael Wolff[3], Jason W. T. Hessels[7,8], Cees G. Bassa[7], Evan F. Keane[9], Elizabeth C. Ferrara[10], Alice K. Harding[10], and Kent S. Wood[3]

[1] Jodrell Bank Centre for Astrophysics, School of Physics and Astronomy, University of Manchester, M13 9PL, UK
[2] National Centre for Radio Astrophysics, Tata Institute of Fundamental Research, Pune 411 007, India
[3] Space Science Division, Naval Research Laboratory, Washington, DC 20375-5352, USA
[4] NRC Research Associate, resident at Naval Research Laboratory, Washington, DC 20375-5352, USA
[5] Columbia Astrophysics Laboratory, Columbia University, New York, NY 10027, USA
[6] College of Science, George Mason University, Fairfax, VA 22030, USA, resident at Naval Research Laboratory, Washington, DC 20375, USA
[7] ASTRON, the Netherlands Institute for Radio Astronomy, Postbus 2, 7990 AA, Dwingeloo, The Netherlands
[8] Anton Pannekoek Institute for Astronomy, University of Amsterdam, Science Park 904, 1098 XH Amsterdam, The Netherlands
[9] Centre for Astrophysics and Supercomputing, Swinburne University of Technology, Mail H30, P.O. Box 218, VIC 3122, Australia
[10] NASA Goddard Space Flight Center, Greenbelt, MD 20771, USA

ABSTRACT

XSS J12270−4859 is an X-ray binary associated with the *Fermi* Large Area Telescope gamma-ray source 1FGL J1227.9−4852. In 2012 December, this source underwent a transition where the X-ray and optical luminosity dropped and the spectral signatures of an accretion disk disappeared. We report the discovery of a 1.69 millisecond pulsar (MSP), PSR J1227−4853, at a dispersion measure of $43.4\,\mathrm{pc\,cm^{-3}}$ associated with this source, using the Giant Metrewave Radio Telescope (GMRT) at 607 MHz. This demonstrates that, post-transition, the system hosts an active radio MSP. This is the third system after PSR J1023+0038 and PSR J1824−2452I showing evidence of state switching between radio MSP and low-mass X-ray binary states. We report timing observations of PSR J1227−4853 with the GMRT and Parkes, which give a precise determination of the rotational and orbital parameters of the system. The companion mass measurement of 0.17–$0.46\,M_\odot$ suggests that this is a redback system. PSR J1227−4853 is eclipsed for about 40% of its orbit at 607 MHz with additional short-duration eclipses at all orbital phases. We also find that the pulsar is very energetic, with a spin-down luminosity of $\sim 10^{35}\,\mathrm{erg\,s^{-1}}$. We report simultaneous imaging and timing observations with the GMRT, which suggests that eclipses are caused by absorption rather than dispersion smearing or scattering.

Key words: accretion, accretion disks – binaries: eclipsing – pulsars: individual (PSR J1227–4853) – X-rays: binaries

1. INTRODUCTION

Neutron star low-mass X-ray binaries (LMXBs) and radio millisecond pulsars (MSPs) are evolutionarily linked, where MSPs are the end products of an episode of accretion of matter and angular momentum from the binary companion to the neutron star (Bhattacharya & van den Heuvel 1991). Recent observations of PSR J1023+0038 (Takata et al. 2013; Patruno et al. 2014; Stappers et al. 2014) and PSR J1824−2452I (Papitto et al. 2013) have directly shown transitions from LMXB to MSP states and vice versa. Such systems in tight orbits ($\lesssim 1$ day) around main-sequence-like companions (with typical mass 0.2–$0.3\,M_\odot$) are called "redbacks" (Roberts 2011), similar to another class of eclipsing systems, called "black-widows," containing MSPs that are ablating their very low-mass ($<0.05\,M_\odot$) companions (Bhattacharyya et al. 2013). The discovery of more such LMXB–MSP systems will help to determine whether they are on the way to becoming canonical MSPs with white dwarf companions, or whether they are a subclass of MSPs that will continue to transition back and forth between the two states.

PSR J1023+0038 was the first such system seen to transition from an LMXB to an eclipsing binary radio MSP (Archibald et al. 2009). PSR J1023+0038 disappeared as an observable radio MSP sometime in 2013 June (Stappers et al. 2014), suggesting a return to the LMXB state. Patruno et al. (2014)

reported that an accretion disk has recently formed in the system and also reported the detection of fast X-ray changes spanning about two orders of magnitude in luminosity. PSR J1023+0038 has also brightened by a factor of ∼5 in gamma rays since the radio pulsations disappeared (Stappers et al. 2014). The only other known gamma-ray-emitting LMXB is XSS J12270−4859, which is positionally coincident with the *Fermi* gamma-ray source 1FGL J1227.9−4852. Based on this coincidence and similarities with PSR J1023+0038, XSS J12270−4859 was expected to be another system capable of transitioning to a radio MSP state (Hill et al. 2011).

A sudden decrease of optical and X-ray brightness for XSS J12270−4859 between 2012 November 14 and 2012 December 21 was reported by Bassa et al. (2014). The optical flux decreased by 1.5–2 mag, while the *Swift* X-Ray Telescope count rate decreased by at least a factor of 10 over the same time period. The previous signs of an accretion disk (i.e., double-peaked optical emission lines) also disappeared. *Chandra* and *XMM-Newton* observations presented by Bogdanov et al. (2014) showed a (previously absent) orbital modulation of the X-ray brightness which, in analogy to PSR J1023+0038, is believed to come from an active pulsar wind shocking near the surface of the companion star (Bogdanov et al. 2011). The XSS J12270−4859 observations suggested a transition from an LMXB-like state in 2012 to one where the

accretion disk was absent in 2013. A faint non-thermal radio source was identified in the field of XSS J12270−4859 (Masetti et al. 2006; Hill et al. 2011). However, the flat spectral index of this emission seen during the LMXB state was probably caused by an outflow rather than radio pulsar emission, which is also reported for PSR J1023+0038 (Deller et al. 2014). Bassa et al. (2014) had searched for radio pulsations using the Parkes at 1.4 GHz, but pulsations were not found in a blind search. This Letter describes the radio pulsar discovery with the GMRT and the follow-up study of PSR J1227−4853, the redback MSP associated with XSS J12270−4859.

2. RADIO OBSERVATIONS AND SEARCH ANALYSIS

We searched for radio millisecond pulsations in XSS J12270−4859 with the Giant Metrewave Radio Telescope (GMRT) at 607 MHz. The GMRT Software Back-end (Roy et al. 2010) produces simultaneous incoherent and coherent beam filter-bank outputs of 512 × 0.0651 MHz channels at 61.44 μs. We performed sensitive coherent array observations using 70% of the GMRT array (Roy et al. 2012) with phase center at R.A. = 12^{h}27^{m}58^{s}8, Decl. = −48°53′42″1 (Masetti et al. 2006). We recorded three 1 hr long scans, beginning on 2014 February 12 at 20:46:15 UTC, interleaving with phase calibrator scans once an hour.

We processed the data in six half-hour segments on the NCRA IBM cluster with Fourier-based acceleration search methods implemented in PRESTO (Ransom et al. 2002). We investigated trial dispersion measures (DMs) ranging from 0 pc cm^{-3} up-to 500 pc cm^{-3}. The Fourier-based periodicity search was done using harmonic summing up to eight harmonics. Considering 32 MHz bandwidth, 10% duty cycle, and a coherent array gain of ∼7 K Jy^{-1}, for a 30 minute observing time we estimate the search sensitivity as (92 K +T_{sky})/(1020 K) mJy for a 5-σ detection at 607 MHz. Considering T_{sky} ∼ 10 K (Haslam et al. 1981), our search sensitivity is ∼0.1 mJy.

In the first 30 minute period, we discovered a highly accelerated 1.69 ms pulsar at a DM of 43.4 pc cm^{-3} (reported in Roy et al. 2014).

3. FOLLOW-UP RADIO TIMING

Following the discovery we started a timing campaign for PSR J1227−4853 using the GMRT coherent array at 607 MHz. We also have a few detections of this pulsar at 322 MHz using the GMRT and at 1.4 GHz using the Parkes telescope.The timing observations span 270 days, from 2014 February 20 to November 17, consisting of 25 epochs, each typically 1 hr long. The filter-bank settings defined in Section 2 were used for both the GMRT bands. The Parkes observations used the DFB3 pulsar backend producing 512 × 0.5 MHz channels at 80 μs. The left panel of Figure 1 shows the orbital phases of our observations. The pulsar is not detected between orbital phases of 0.05 and 0.45 (phase 0.25 is superior conjunction of the pulsar) and there are also frequent intervals of non-detections well outside the main eclipsing region, which is quite similar to what is seen in PSR J1023+0038 (Archibald et al. 2013). We used multi-Gaussian fits to high signal-to-noise observations at each frequency to produce templates that were used for extracting times of arrival (TOAs). Typically, 10 TOAs were derived from each observing session.

Using the 2MASS catalog position of R.A. = 12^{h}27^{m}58^{s}748, Decl. = −48°53′42″88 (J2000; Masetti et al. 2006; Cutri 2013), for the a priori astrometric model and the JPL DE405 solar system ephemeris (Standish 2004), we obtained a phase-connected timing model using TEMPO.[11] We used a constant offset between the Parkes and the GMRT TOAs of 0.542 ms, which was measured using the global timing campaign data of PSR J1713+0747 taken simultaneously at a similar observing frequency (Dolch et al. 2014). The global timing ephemeris having precise DM measured for that epoch was used to estimate this JUMP, which absorbs any fixed time offsets between the different backends and observatory clocks. The DM was determined using 607 MHz GMRT TOAs and 1.4 GHz Parkes TOAs excluding the orbital phases 0.0–0.5. The binary timing model used is ELL1 (Lange et al. 2001). Since we do not measure a significant eccentricity (with an upper limit of $e < 3.3 \times 10^{-5}$), we set the eccentricity to zero in our timing model. The best-fit timing model (given in Table 1) is obtained for 270 days of data excluding the TOAs around the main eclipse phase and achieved a post-fit rms timing residual of 10 μs (Figure 2).

The eclipse region is symmetrical around the orbital phase 0.25 with a duration of around 2.7 hr (40% of the orbital period). The companion's Roche lobe radius of 0.24 $R_{\odot}$ is much smaller than the opaque portion of the companion's orbit (4.9 $R_{\odot}$), indicating that ionized material lies far outside the Roche lobe causing excess DM at the eclipse boundaries. The excess DM of 0.013 pc cm^{-3} seen at the eclipse ingress (as seen in Figure 2) corresponds to an added electron density of >4 × 10^{16} cm^{-2}.

4. RADIO IMAGING AND FLUX VARIATIONS

The GMRT interferometric visibility measurements allowed us to carry out continuum imaging of the field of PSR J1227−4853. We used the observation on 2014 February 20 taken at 607 MHz for imaging studies, where the pulsar was tracked from rise to set, resulting in 3.5 hr of on-source time recorded in multiple scans. In this time interval, the pulsed emission is seen only for the last 43 minutes of the observation, corresponding to orbital phases of 0.48–0.57. The raw data were converted into FITS format, after which they were processed by the flagging and calibration pipeline flagcal (Prasad & Chengalur 2012; Chengalur 2013). Flux, phase, and bandpass calibration were done using nearby calibrator, J1154–3505. The interpolated flux at 607 MHz was computed to be 7.9 Jy using the Very Large Array calibrator manual. All further processing was done using AIPS.[12]

Self-calibration was done using 30″ × 21″ resolution faceted images of the field made using the three-dimensional imaging option of IMAGR. A full resolution image of only the region around the target source was made separately for each of the scans. Emission in the region of the target source was seen only in the last scan (image in Figure 3), which corresponds to the time interval where the pulsed emission is seen in the synchronously taken TOAs. The position and peak flux measured from Gaussian fitting to the source are R.A. (2000) = 12^{h}27^{m}58^{s}4 ± 0^{s}3, decl. (2000) = −48°53′44″3 ± 2″5, and 6.6 ± 0.2 mJy, respectively. A light curve for this source was then determined by making images at 1 minute
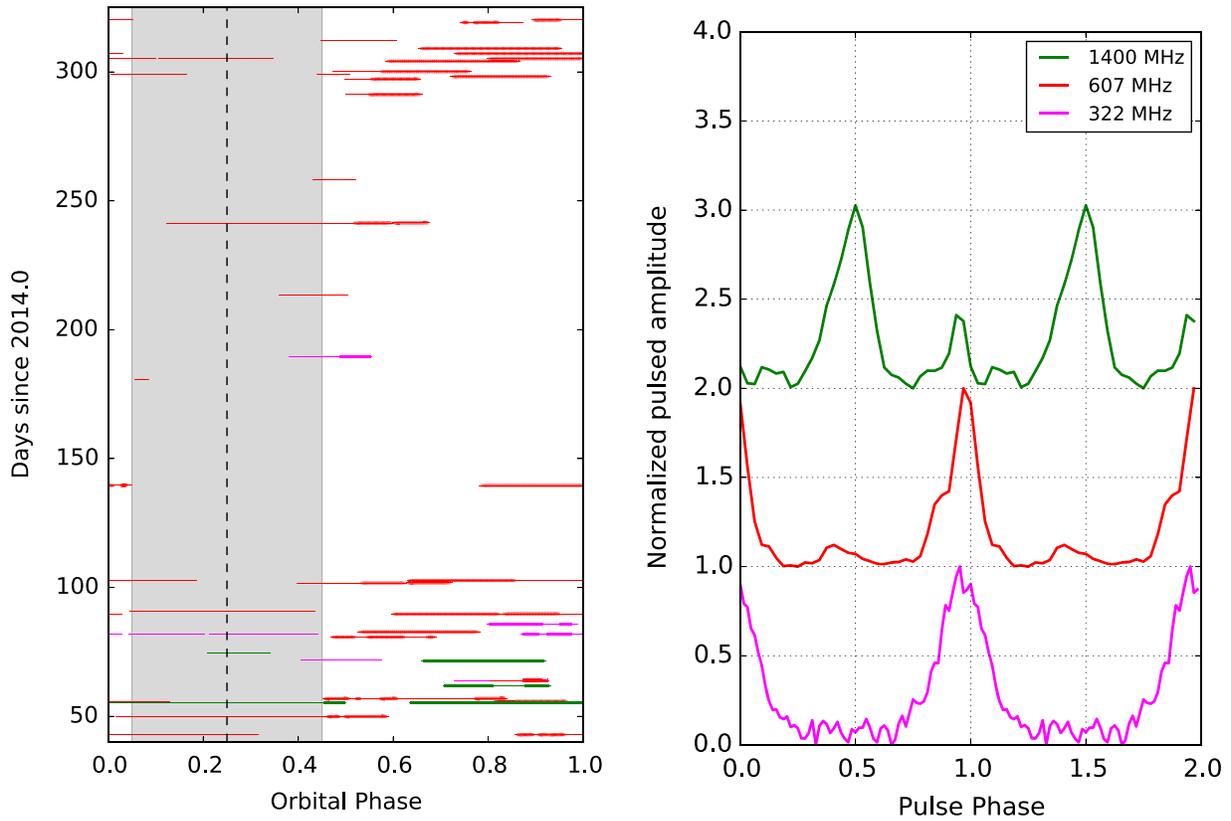

Figure 1. Left panel: orbital phase coverage, where thick lines indicates detections. Red and magenta symbols correspond to GMRT observations at 607 and 322 MHz, respectively, and green for Parkes observations at 1.4 GHz. The eclipse region is shaded and the superior conjunction is marked by the dotted line. Right panel: pulse profiles at three observing frequencies with vertical offsets added for clarity. GMRT–Parkes time offset and the profile evolution can make the profile alignment covariant with DM.
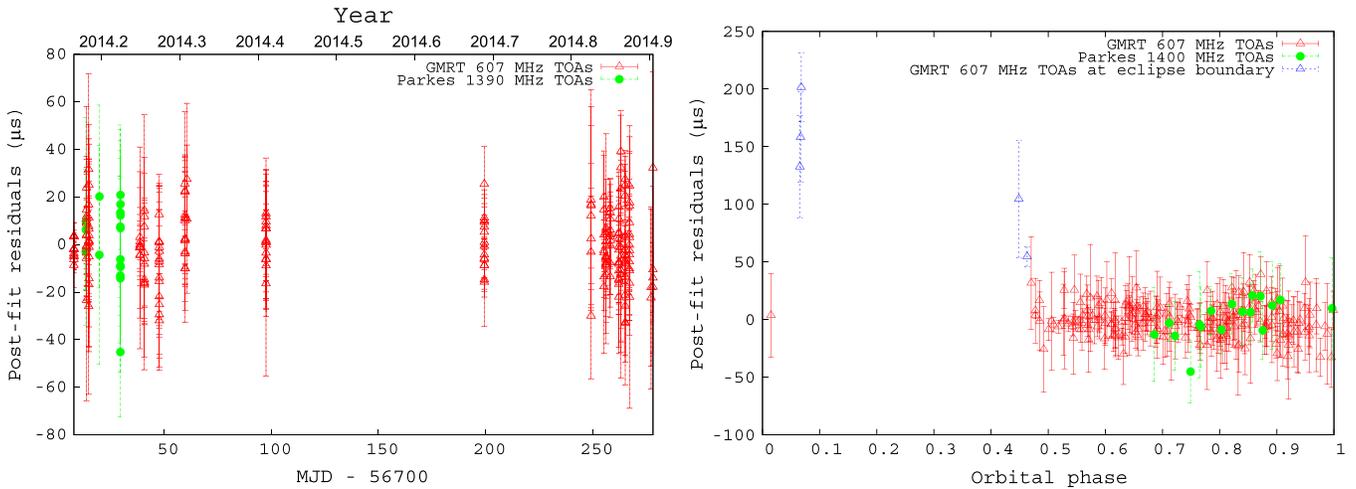

Figure 2. Post-fit timing residuals of PSR J1227−4853 as a function of MJD (left panel) and binary phase (right panel). The large 100 day gap in the TOAs is caused by the observations at eclipsing binary phase on 56838 and 56871 MJD. The 607 MHz TOAs are marked as red open triangles and the 1390 MHz TOAs are marked as green circles; 607 MHz TOAs at the eclipse boundary are included only in the right panel plot (to illustrate the excess delay), but not in the timing fit.

resolution. Figure 3 compares the continuum flux variation with the mean pulsed flux and the pulse arrival time delays as a function of orbital phase.

During the main eclipse phase no emission is seen at the pulsar location. To place the best possible limit, all of the detected sources, except from the central facet, were subtracted from the visibility data. A further round of self-calibration was done using only the sources in the central facet, providing a better correction for the ionospheric phases. The final rms noise

that we achieve is $85\,\mu$Jy using the data for the full eclipse duration. Hill et al. (2011) reported the detection of a continuum source (at an epoch which corresponds to the X-ray accreting phase) at the location of the pulsar with a flux of $190\,\mu$Jy at 9 GHz and a spectral index of -0.1 ± 0.1 (based on reanalysis by Bassa et al. 2014). Though our non-detection is consistent with the nominal spectral index, the emission observed by Hill et al. (2011) could be powered by an outflow, which is absent in the GMRT image, as the outflow

Table 1
Parameters of PSR J1227−4853

Parameter	Value[a]
2MASS Position[b]	
R.A. (J2000)	$12^h27^m58\overset{s}{.}748 \pm 0\overset{s}{.}06$
Decl. (J2000)	$-48°53'42\overset{''}{.}88 \pm 1\overset{''}{.}$
Parameters From Radio Timing	
R.A. (J2000)	$12^h27^m58\overset{s}{.}724(1)$
Decl. (J2000)	$-48°53'42\overset{''}{.}741(3)$
Pulsar frequency f (Hz)	592.987773605(4)
Frequency derivative $\dot{f}$ (Hz s^{-1})	$-3.9\,(4) \times 10^{-15}$
Period epoch (MJD)	56707.9764
Dispersion measure DM (cm^{-3} pc)	43.4235(7)
Binary model	ELL1
Orbital period P_b (days)	0.287887519(1)
Orbital period derivative $\dot{P}_b$	$-8.7(1) \times 10^{-10}$
Projected semimajor axis x (lt-s)	0.668468(4)
Epoch of ascending node passage T_{ASC} (MJD)	56700.9070772(2)
Span of timing data (MJD)	56707.95−56978.13
Number of TOAs	236
Post-fit residual rms (μs)	10.1
TOA error scale factor[c]	2.5
Reduced chi-square	0.58
Derived Parameters	
Mass function f ($M_\odot$)	0.00386973
DM distance[d] (kpc)	1.4
Flux density at 607 MHz[e] (mJy)	6.6(2)
Surface magnetic field B_s (10^8 G)	1.36(6)
Spin down luminosity $\dot{E}$ (10^{35} erg s^{-1})	0.90(8)
Characteristic age τ (Gyr)	2.4(2)

[a] Errors in the last digit are in parentheses.
[b] Cutri (2013).
[c] TOA uncertainties were multiplied by EFAC to correct for generally underestimated uncertainty produced by TEMPO.
[d] Cordes & Lazio (2002).
[e] Measured with continuum imaging. Differs from the preliminary estimate of Roy et al. (2014), likely due to an un-calibrated coherent array gain and possible scintillation effects.

driven radio emission turns off during radio MSP state (Bassa et al. 2014).

5. PRE-DISCOVERY RADIO OBSERVATIONS

Prior to the discovery of PSR J1227−4853, several searches for radio pulsations have been attempted using Parkes and GMRT. All of them (listed in Table 2) resulted in non-detections. We compute the pulsed flux density limits using nominal telescope parameters such as gain, bandwidth, etc (Ray et al. 2011, Table 19). We consider a pulse duty cycle of 10% and a 5σ detection threshold. Parkes 1390 MHz on 2012 March 22 and GMRT 322 MHz on 2012 July 23 are the only two observations spanning the non-eclipsing binary phases of the pulsar during the LMXB state. There is a marginal 5σ detection of pulsation for the 2012 March 22 Parkes observations, when folded with the radio timing ephemeris. We also folded the Parkes data from Bassa et al. (2014) and detected the pulsar in several intervals of the 2013 November 13 observation (details in Table 2) at 1390 MHz, at a significance below the threshold used for their blind search.

6. DISCUSSION

We report the GMRT discovery of a redback MSP, PSR J1227−4853, associated with the LMXB system XSS J12270−4859, confirming that the system now hosts an active radio MSP as predicted by Bassa et al. (2014). This is the third system after PSR J1023+0038 and PSR J1824−2452I showing evidence of state switching between the LMXB and MSP states. We report results from radio timing observations with the GMRT and Parkes spanning over 270 days from 2014 February 20 to November 17. Comparing TOAs derived from the 2013 November 13 Parkes observation from Bassa et al. (2014) indicates $\sim$2 s change in T_{ASC} relative to the extrapolation of our timing model. This is similar to orbital phase changes seen in PSR J1023+0038 by Archibald et al. (2013). A model with up to third-order orbital period derivatives is required to accommodate such a rapid change, similar to what is observed in PSR J2051−0827 (Lazaridis et al. 2011).

Based on our radio timing, we measure $P_b = 0.287887519$ (1) days and obtain the first detection of $\dot{P}_b = -8.7(1) \times 10^{-10}$. Though the P_b determined from radio timing is consistent at the 2σ level with the photometric period of 0.28804(8) days from Bassa et al. (2014), our measurement differs by 0.000132(2) days from the spectroscopic P_b measurement of 0.2880195(22) days by de Martino et al. (2014) obtained in 2012 March/April and 2013 December. This difference can not be explained by the observed $\dot{P}_b$. Instead, it appears de Martino et al. (2014) miscounted the number of orbital revolutions between their observations. The zero-crossing time (T_0) from de Martino et al. (2014) show that their spectroscopic P_b counts 2172 orbital revolutions, one revolution less when using the more accurate and correct P_b derived from pulsar timing.

Converting the $T0$ measurements by de Martino et al. (2014) from HJD to TDB, we find that the radio timing ephemeris provides orbital phases (ϕ) of 0.244(6) and 0.263(17) for the 2012 March/April and 2013 December epochs. These correspond to inferior conjunction of the companion star, which is consistent with the T_{ASC} used in the timing ephemeris. Our timing ephemeris yields an ϕ of 0.997(7) for the zero phase of the photometric light curve given in Bassa et al. (2014). Note that time-definition in Bassa et al. (2014) is in error; it is TDB instead of HJD (C. Bassa 2015, private communication). In conclusion, the optical phase measurements by Bassa et al. (2014) and de Martino et al. (2014) are consistent with our timing ephemeris of a pulsar orbiting an irradiated binary companion.

The timing ephemeris also provides the projected radial velocity amplitude of the pulsar $K_1 = 50.622619464$ (1) km s^{-1}. Combined with the projected radial velocity amplitude of the companion determined from optical spectroscopy, $K_2 = 261(5)$ km s^{-1} (de Martino et al. 2014), this constrains the mass ratio to $q = M_2/M_1 = 0.194(3)$. For an edge-on orbit, the measurement of the mass ratio and the mass functions set 1σ lower limits on the mass of the companion and the pulsar as 0.142 and 0.719 $M_\odot$, respectively. Further constraints are provided by limiting the orbital inclination to $i \gtrsim 43°$ (de Martino et al. 2014). The absence of X-ray eclipses leads these authors to suggest $i \lesssim 73°$. For this range in inclination the companion mass is constrained to 0.167−0.462 $M_\odot$, while the pulsar has a mass of 0.86−2.38 $M_\odot$. The combination of q and K_2, allows an estimate of the rotational broadening of spectral lines of the
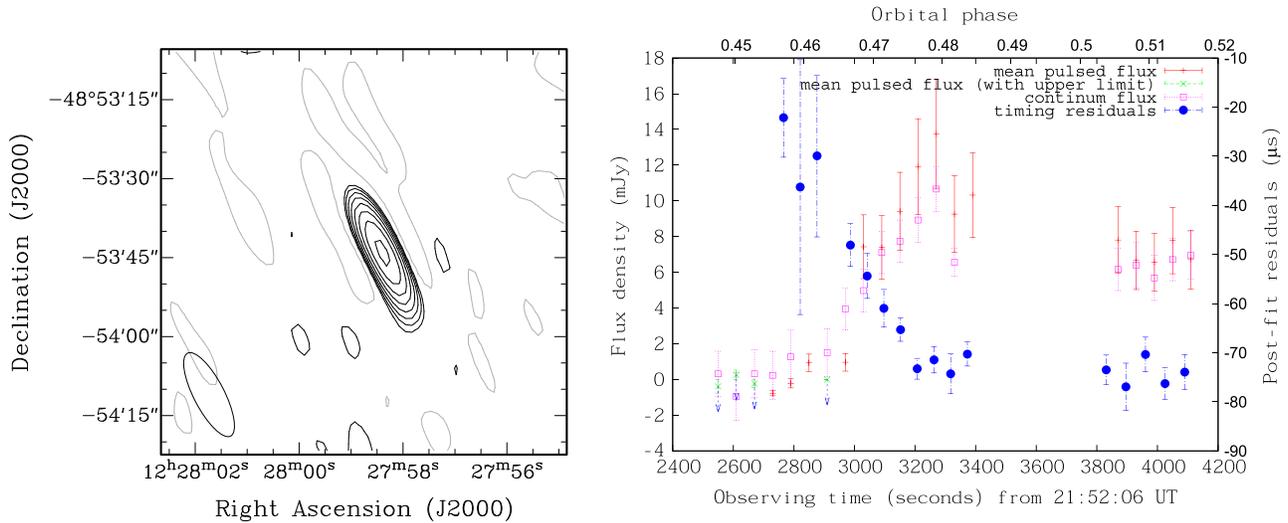
Figure 3. Left panel: radio emission at 607 MHz at the location of PSR J1227–4853 from the GMRT observations over the orbital phase of 0.48–0.57. Contours start at 0.5 mJy/beam and increase in steps of $\sqrt{2}$. The 2σ negative contour is shown in gray. The synthesized beam (lower left corner) is $15'' \times 5''$. Right panel: variation of flux density at the eclipse egress. Continuum fluxes are plotted in purple and mean pulsed fluxes are plotted in red. Upper limits in mean pulsed flux density are given in case of non-detections. Timing residuals (right side y-axis) at the eclipse egress is plotted in blue. There is a gap in the data between 3400–3800 s due to scan boundaries.

Table 2
Pre-discovery Radio Pulsation Search Observations

Telescope	Frequency (MHz)	Date	$t_{\rm obs}$ (h)	Orbital Phase	$S_{\rm min}$[a] (mJy)
Parkes	1390	2009 Nov 25[b]	2	0.12–0.41	0.15
Parkes	1390	2010 Jul 18[b]	1.1	0.05–0.21	0.20
Parkes	1390	2010 Nov 12[b]	1	0.25–0.40	0.21
Parkes	1390	2012 Mar 22	1	0.78–0.92	0.21
GMRT[c]	322	2012 Jul 23	1	0.88–0.02	0.09
Parkes	1390	2012 Nov 07	0.75	0.16–0.2	0.25
Parkes	1390	2013 Nov 13[d]	1	0.43–0.57	0.20
Parkes	1390	2013 Nov 13[d],*	1	0.58–0.72	0.20
Parkes	1390	2013 Nov 13[d],*	1	0.73–0.87	0.20
Parkes	1390	2013 Nov 13[d],*	1	0.87–0.02	0.20
Parkes	1390	2013 Nov 13[d]	1	0.02–0.16	0.20
Parkes	1390	2013 Nov 17[d]	1	0.48–0.62	0.20
Parkes	1390	2014 Jan 09[d]	1	0.79–0.93	0.20
Parkes	3100	2014 Jan 09[d]	0.58	0.96–0.04	0.54
Parkes	732	2014 Jan 09[d]	0.58	0.96–0.04	0.19

Notes. Back ends used for Parkes observations: up to 2012 using AFB; 2013 and 2014 observations at 1390 MHz using BPSR; DFB3 and DFB4 for 732 and 3100 MHz, respectively.
[a] $S_{\rm min}$ is quoted for 607 MHz using spectral index of −1.7.
[b] Hill et al. (2011).
[c] Incoherent array mode.
[d] Bassa et al. (2014), * with detections.

companion through $v_{\rm rot} \sin i = 0.46 K_2 [(1 + q)^2 q]^{1/3} = 78(12)$ km s^{-1}. This implicitly assumes that the companion is filling its Roche lobe and is tidally locked with the binary orbit (Wade & Horne 1988). This prediction of the rotational broadening is consistent with the measured value of $v_{\rm rot} \sin i = 86(20)$ km s^{-1} during the LMXB state (de Martino et al. 2014; though the rotational broadening is close to the instrumental resolution), suggesting that the binary companion of PSR J1227–4853 was (or was close to) filling its Roche lobe prior to the 2012 transition. Modeling of the light curves for companion stars of other redbacks has also shown them to be (near) Roche lobe filling (Breton et al. 2013).

We also report a spin-down luminosity, $\dot{E} = 0.9 \times 10^{35}$ erg s^{-1}, which is $\sim 10^3$ times the X-ray luminosity in the MSP state. This places PSR J1227–4853 among the few highly energetic MSPs with $\dot{E} \sim 10^{35}$ erg s^{-1}. The Shklovskii correction for $\dot{P}$ considering a typical MSP velocity (85 km s^{-1}; Toscano et al. 1999) is <1%. The measured $\dot{E}/a^2$ (= $\sim 4.3 \times 10^{33}$ erg lt-s^{-2} s^{-1}), where a (= $1.97 R_\odot$) is the separation between the pulsar and companion, is indicative of greater energy flux of the system (and is similar to that of PSR J1023+0038) to efficiently drive off material from the surface of the companion.

The simultaneous timing and imaging studies of PSR J1227–4853 provide a powerful probe of the eclipse mechanism. The very well correlated variation of continuum flux density and mean pulsed flux density at the eclipse boundary helps to rule out effects such as excess dispersion or scattering being the cause of eclipse. Rather, cyclotron–synchrotron absorption of the radio waves by electrons is likely to be the cause of the radio eclipse (Thompson et al. 1994).

Since the discovery of PSR J1227–4853, we have radio timing observations at the GMRT spanning 270 days, where the MSP is consistently bright. Thus, it is clear that the pulsar has transitioned from an accreting state around the end of 2012 and is now in a radio MSP state for at least 362 days (including the 2013 November 13 detections). The marginal detection of radio pulsations in 2012 may suggest that the system had entered a propeller state possibly alternating with a rotational-powered state on short timescales (Patruno et al. 2013). The discovery of radio pulsations in XSS J12270–4859 further establishes that the sudden decrease in X-ray and optical flux (as well as the disappearance of double-peaked emission lines) relates to a cessation of accretion in the system, which has now firmly transitioned to a radio MSP state. Considering the recent reverse swing from MSP to LMXB state in PSR J1023+0038, PSR J1227–4853 may also return back to the LMXB state within the coming year(s), resulting in the disappearance of radio pulsations. Then it will be possible to study what type of accretion state the system enters and whether material is being channeled onto the neutron star (Archibald et al. 2014; Papitto et al. 2014).

REFERENCES

Archibald, A. M., Stairs, I. H., Ransom, S. M., et al. 2009, Sci, 324, 1411
Archibald, A. M., Kaspi, V. M., Hessels, J. W. T., et al. 2013, arXiv:1311.5161
Archibald, A. M., Bogdanov, S., Patruno, A., et al. 2014, arXiv:1412.1306
Bassa, C. G., Patruno, A., Hessels, J. W. T., et al. 2014, MNRAS, 441, 1825
Bhattacharya, D., & van den Heuvel, E. P. J. 1991, PhR, 203, 1
Bhattacharyya, B., Roy, J., Ray, P. S., et al. 2013, ApJL, 773L, 12B
Bogdanov, S., Archibald, A. M., Hessels, J. W. T., et al. 2011, ApJ, 742, 97
Bogdanov, S., Patruno, A., Archibald, A. M., et al. 2014, ApJ, 789, 40
Breton, R. P., van Kerkwijk, M. H., Roberts, M. S. E., et al. 2013, ApJ, 769, 108
Chengalur, J. N. 2013, NCRA Technical Report, NCRA/COM/001

Cordes, J. M., & Lazio, T. J. W. 2002, arXiv:astro-ph/0207156
Cutri, R. M., Skrutskie, M. F., van Dyk, S., et al. 2003, yCat, 2246, 0
Deller, A. T., Moldón, J., Miller-Jones, J. C. A., et al. 2014, arXiv:1412.5155
de Martino, D., Casares, J., Mason, E., et al. 2014, MNRAS, 444, 3004
Dolch, T., Lam, M. T., Cordes, J., et al. 2014, ApJ, 794, 21
Haslam, C. G. T., Klein, U., Salter, C. J., et al. 1981, A&A, 100, 209
Hill, A. B., Szostek, A., Corbel, S., et al. 2011, MNRAS, 415, 235
Lange, C., Camilo, C., Wex, N., et al. 2001, MNRAS, 326, 274
Lazaridis, K., Verbiest, J. P. W., Tauris, T. M., et al. 2011, MNRAS, 414, 3144
Masetti, N., Morelli, L., Palazzi, E., et al. 2006, A&A, 459, 21
Papitto, A., Ferrigno, C., Bozzo, E., et al. 2013, Natur, 501, 517
Papitto, A., de Martino, D., Belloni, T. M., et al. 2014, arXiv:1412.4252
Patruno, A., & D'Angelo, C. 2013, ApJ, 771, 94
Patruno, A., Archibald, A. M., Hessels, J. W. T., et al. 2014, ApJ, 781, 3
Prasad, J., & Chengalur, J. 2012, ExA, 33, 157
Ransom, S. M., Eikenberry, S. S., & Middleditch, J. 2002, AJ, 124, 1788
Ray, P. S., Kerr, M., Parent, D., et al. 2011, ApJS, 194, 17
Roy, J., Bhattacharyya, B., & Gupta, Y. 2012, MNRASL, 27, 90
Roy, J., Bhattacharyya, B., & Ray, P. 2014, ATel, 5890, 1
Roy, J., Gupta, Y., Ue-Li Pen, et al. 2010, ExA, 28, 25
Roberts, M. S. E. 2011, in AIP Conf. Proc., 1357, 40
Standish, E. M. 2004, A&A, 417, 1165
Stappers, B. W., Archibald, A. M., Hessels, J. W. T., et al. 2014, ApJ, 790, 39
Takata, J., Li, K. L., Leung Gene, C. K., et al. 2014, ApJ, 785, 131
Thompson, C., Blandford, R. D., Evans, C. R., & Phinney, E. S. 1994, ApJ, 422, 304
Toscano, M., Sandhu, J. S., Bailes, M., et al. 1999, MNRAS, 307, 925
Wade, R. A., & Horne, K. 1988, ApJ, 324, 411

6